IAC-14-C1.2.2

DENSITY EVOLUTION OF HIGH AREA-TO-MASS OBJECTS USING SEMI-ANALYTICAL AND DIFFERENTIAL ALGEBRA TECHNIQUES

Alexander Wittig
Department of Aerospace Science and Technology, Politecnico di Milano, Milano, Italy; alexander.wittig@polimi.it

Camilla Colombo
Department of Aerospace Science and Technology, Politecnico di Milano, Milano, Italy; camilla.colombo@polimi.it

Roberto Armellin
Aeronautics, Astronautics and Computational Engineering Research Unit, University of Southampton, Southampton, UK; roberto.armellin@soton.ac.uk

This paper introduces and combines two novel techniques. Firstly, we introduce an efficient numerical method for the propagation of entire sets of initial conditions in the phase space and their associated phase space densities based on Differential Algebra (DA) techniques. Secondly, this DA density propagator is applied to a DA-enabled implementation of Semi-Analytical (SA) averaged dynamics, combining for the first time the power of the SA and DA techniques.
While the DA-based method for the propagation of densities introduced in this paper is independent of the dynamical system under consideration, the particular combination of DA techniques with SA equations yields a fast and accurate method to propagate large clouds of initial conditions and their associated probability density functions very efficiently for long time. This enables the study of the long-term behavior of particles subjected to the given dynamics.
To demonstrate the effectiveness of the proposed method, the evolution of a cloud of high area-to-mass objects in Medium Earth Orbit is reproduced considering the effects of solar radiation pressure, the Earth's oblateness and luni-solar perturbations. The computational efficiency is demonstrated by propagating $10,000$ random samples taking snapshots of their state and density at evenly spaced intervals throughout the integration. The total time required for a propagation for 16 years in the dynamics is on the order of tens of seconds on a common desktop PC.

I. INTRODUCTION

Differential Algebra (DA) is a well established tool for the propagation of clouds of initial conditions through any sufficiently smooth dynamical system [1, 2]. It allows the fast and efficient computation of a high order polynomial expansion of the final state as a function of the initial state. As such, it provides a method for the propagation of uncertainties with a single integration [2]. Besides the huge reduction in computational cost compared to many pointwise integrations, another advantage of DA over conventional pointwise integration is the fact that it yields an analytical expression which approximates the dependence on initial conditions and system parameters.

One of the novel results of this work is that we show how the information contained in the DA flow expansion can be used to not only to propagate points, but also to automatically propagate a probability density function in time at no extra cost. As is the case with the DA propagation method, the DA density propagator is agnostic with respect to the dynamics, i.e. it can be used to propagate densities in arbitrary dynamical systems without requiring additional information. In particular, it is not necessary to derive and integrate e.g. variational equations. The result of the DA density propagation is an expansion of the metric tensor used to transform the probability density function. As such, it permits the efficient propagation of an arbitrary initial probability density function through the dynamics by the mere evaluation of a polynomial as opposed to repeated pointwise integrations.

An area of astrodynamics where the propagation of densities is of particular interest is the long term evolution of orbits around a primary body. When analyzing the long-term evolution and stability of the motion of natural or artificial satellites in a planet-centered dynamics, the effect of orbit perturbations is fundamental. Solar radiation pressure and planetary oblateness are essential to predict the motion of impact ejecta from Phobos and Deimos in orbits around Mars [3] or high area-to-mass spacecraft around the Earth [4]. Similarly, the space debris evolution environment models implement the effect of solar radiation pressure, third body perturbations of Sun and Moon, and the effect of the Earth's oblateness [5].

An elegant approach to analyze the effect of orbit perturbations is the Semi-Analytical (SA) technique based on averaging, which separates the constant, short periodic and long-periodic terms of the disturbing function. The short-term effect of perturbations is eliminated by averaging the variational equations or the corresponding potential over one orbit revolution of the small body. Indeed, averaging corresponds to filtering the higher frequencies of the motion (periodic over one orbit revolution), which typically have small amplitudes. The resulting equations often permit a deeper understanding of the dynamics [6], and to identify equilibrium solutions, librational or rotational solutions [4]. From a numerical point of view, the advantage of the SA approach lies in the reduced computational cost of the dynamics as the stiffness of

the problem is reduced, while maintaining sufficient accuracy compatible with problem requirements also for long-term integrations.

Semi-analytical and various Differential Algebra based techniques were previously compared for the long term propagation [7]. In particular, a comparison was performed between the direct integration of the full high fidelity equations of motion using DA and the averaged equations developed for the long term propagation of spacecraft in the Earth's environment [8]. DA was successfully employed to propagate an initial set comprised of tens of thousands of initial conditions. The combination of DA with semi-analytical techniques demonstrated great potential in reducing the computational time.

In this paper we continue our work on combining DA integration techniques with the SA equations of motion. We implement DA enabled SA dynamical models for high area-to mass objects expressed in terms of secular variation of the Keplerian orbital elements, taking into account solar radiation pressure, the Earth's oblateness and perturbations due to luni-solar gravity. These dynamics are then used with the DA density propagator to represent the evolution of a cloud of high area-to-mass fragments in Medium Earth Orbit (MEO). In particular, the density evolution is shown in the phase space of eccentricity and longitude with respect to the Sun-Earth direction. Indeed this representation provides interesting insight into the underlying characteristics of the dynamics [4]. The evolution of the phase space density of high area-to-mass objects is shown for different initial conditions and using different perturbation models for the dynamics.

While the approach presented in this paper is based on the metric tensor for the propagation of uncertainties, another method employed in previous research uses the continuity equation to describe the evolution of the density in time. In some special cases even an analytical closed form solution is possible. This approach was successfully applied to describe the population of space debris [9] or the evolution of debris objects after a fragmentation event [10], or a cloud of dust particles under the effects of Pointing-Robertson drag [11], or a swarm of satellites-on-a-chip (SpaceChips) around the Earth [12]. The disadvantage of the continuity equation method is that, to be competitive with respect to numerical integration of the corresponding system of ODE, it requires the derivation of a closed-form expression of the evolution of the density, which is not always possible and depends on the particular dynamics to be considered. However, once obtained, the resulting equation can be evaluated directly at the time where the value of the density is needed. The DA density propagation method presented in this paper does not suffer from the drawbacks of the continuity equation approach as it is agnostic to the dynamics and comes at no additional computational cost as it utilizes the information already present in the DA expansion of the flow.

The article is organized as follows: Section II provides a quick overview over the DA technique, while Section III introduces the important concept of the DA-based high order flow expansion. In Section IV we briefly introduce the averaged dynamics used in this work. Section V introduces the theoretical underpinnings of the density propagation method proposed, while Section VI focuses on the DA implementation aspects of the density propagation. This is followed by various numerical examples in Sections VII–IX. The paper concludes with some conclusion and an outlook on future works.

II. DIFFERENTIAL ALGEBRA

Differential Algebra (DA) techniques, exploited here to implement an automatic high-order density propagation algorithm, were devised to attempt solving analytical problems through an algebraic approach [13]. Historically, the treatment of functions in numerics has been based on the treatment of numbers, and the classical numerical algorithms are based on the mere evaluation of functions at specific points.

DA techniques rely on the observation that it is possible to extract more information on a function rather than its mere values. The basic idea is to bring the treatment of functions and the operations on them to computer environment in a similar manner as the treatment of real numbers. Referring to Figure 1, consider two real numbers a and b. Their transformation into the floating point (FP) computer representation, $\overline{a}$ and $\overline{b}$ respectively, is performed to operate on them in a computer environment. Then, given any operation $*$ in the set of real numbers, an adjoint operation $\circledast$ is defined in the set of FP numbers so that the diagram in Figure 1 (left) commutes[1]. Consequently, transforming the real numbers a and b into their FP representation and operating on them in the set of FP numbers returns the same result as carrying out the operation in the set of real numbers and then transforming the achieved result in its FP representation.

In a similar way, let us suppose two functions f and g in n variables in the space C^k of k times continuously differentiable functions are given. In the framework of differential algebra, the computer represents and operates on them using their k-th order Taylor expansions, F and G respectively. Therefore, the transformation of real numbers into their FP representation is now substituted by the extraction of the k-th order Taylor expansions of f and g. For each operation on C^k, an adjoint operation in the space of truncated Taylor polynomials (called ${}_kD_n$) is defined so that the corresponding diagram commutes; i.e., extracting the k-th order Taylor expansions of f and g and operating on them in ${}_kD_n$ returns the same result as operating on f and g in the original space C^k and then extracting the k-th order Taylor expansion of the resulting function.

The implementation of differential algebra in a computer allows the exact computation of the Taylor coefficients of a function up to a specified order k with a limited amount of effort. The Taylor coefficients of order n for sums and products of functions, as well as scalar products with real numbers, can be computed from the coefficients of the summands and factors. Therefore, the set of equivalence classes of C^k functions can be endowed with well-defined operations, leading to the

[1] The diagram commutes approximately in practice due to truncation errors.

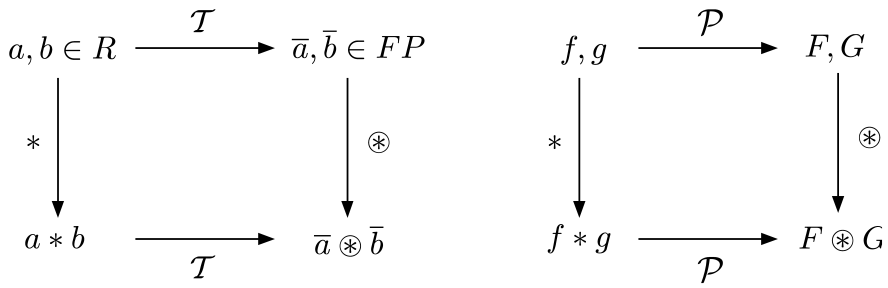

Figure 1: Analogy between the floating point representation of real numbers in a computer environment (left) and the introduction of the algebra of Taylor polynomials in the differential algebraic framework (right).

so-called truncated power series algebra (TPSA) [14, 15]. In addition to these algebraic operations, the DA framework is endowed with differentiation and integration operators, completing the structure of a differential algebra.

Analogously to the algorithms for floating point arithmetic, further algorithms for intrinsic functions are built on these elementary operations yielding common elementary functions, such as trigonometric and exponential functions. Further algorithms to evaluate and perform composition of functions, compute Taylor expansions of inverse functions, and solve nonlinear systems of equations explicitly are available in DA arithmetic [16, 13].

The DA computer routines outlined in this section are implemented in the software COSY INFINITY [17] by M. Berz and K. Makino, which is used in to implement the algorithms presented in this paper.

III. HIGH ORDER FLOW EXPANSION

DA allows the derivatives of any function f of n variables to be computed up to an arbitrary order k. This has an important application to the numerical integration of an ODE by means of an arbitrary numerical integration scheme. Any integration scheme is based on algebraic operations, involving the evaluation of the ODE right hand side at several integration points. Therefore, by carrying out all the evaluations in DA arithmetic allows computing the arbitrary order expansion of the solution of a general ODE with respect to the initial conditions. Throughout the following, the notation $[x]$ is used to represent a DA variable, as opposed to a function or real variable.

To illustrate the method, without loss of generality consider the scalar initial value problem

$$\begin{cases} \dot{x} = f(x,t) \\ x(t_0) = x_0 \end{cases} \tag{1}$$

and the associated flow $\varphi(t;x_0)$ in phase space. We now want to show that, starting from the DA representation of the initial condition x_0, DA allows us to propagate the Taylor expansion of the flow around x_0 forward in time, up to the desired final time t_f, yielding a polynomial expansion of $\varphi(t_f; x_0 + \delta x_0)$.

Initially, at time t_0 the flow $\varphi(t_0;x) = x$ is the identity. We therefore replace the point initial condition x_0 by the DA representation of the identity function expanded around x_0 to order k, which is a $(k+1)$-tuple of Taylor coefficients. As for the identity function only the first two coefficients, corresponding to the constant part and the first derivative respectively, are non zero, we can write $[x_0]$ as $x_0 + \delta x_0$, in which x_0 is the reference point for the expansion.

If all the operations of the numerical integration scheme are now carried out in the DA arithmetic, the flow $\varphi(t;x_0)$ in phase space is approximated, at each time step t_i, as a Taylor expansion in δx_0.

For the sake of clarity, consider the fixed step-size forward Euler's scheme

$$x_i = x_{i-1} + f(x_{i-1})\Delta t \tag{2}$$

and substitute the initial value with the DA identity $[x_0] = x_0 + \delta x_0$. At the first time step we have

$$[x_1] = [x_0] + f([x_0]) \cdot \Delta t. \tag{3}$$

If the function f on the right hand side is evaluated in the DA framework, the output of the first step, $[x_1]$, is the k-th order polynomial expansion of the flow $\varphi(t;x_0)$ in δx_0 around x_0 at time $t = t_1$. Note that, as a result of the DA evaluation of $f([x_0])$, the $(k+1)$-tuple $[x_1]$ may include several non zeros coefficients corresponding to high-order terms in δx_0.

By induction, this procedure can be repeated until reaching the final step, which is the k-th order polynomial expansion of $\varphi(t;x_0)$ in δx_0 around x_0 at the final time $t = t_f$. Thus, the flow of a dynamical system can be approximated, at each time step t_i, as a k-th order Taylor expansion in δx_0 around around x_0 automatically and with a limited amount amount of effort.

In practice, of course, one does not employ a fixed step-size Euler scheme, but a more advanced numerical integration scheme such as higher order Runge-Kutta schemes with automatic step size control or Adams-Bashforth schemes.

The conversion of standard integration schemes to their DA counterparts is straightforward for explicit solvers and if done correctly can also be performed for implicit methods. This is essentially based on the substitution of all the operations in the algorithm by the same operations on DA numbers. In addition, whenever the integration scheme involves iterations (e.g., in implicit and predictor-corrector methods), step size control, and order selection, the usual absolute value must

be replaced by a suitably chosen measure of the accuracy of the Taylor expansion of the flow.

The main advantage of the DA-based approach is that there is no need to write and integrate variational equations in order to obtain high-order expansions of the flow. As this is achieved by the simple substitution of operations between real numbers with those on DA numbers, the method is ODE independent. Furthermore, the efficient implementation of DA in COSY INFINITY allows us to obtain high-order expansions with limited computational time.

For the computations in this paper, we use a $7/8$ order Runge-Kutta integrator scheme with automatic step size control for the integration of the dynamics starting with a DA representation of the initial condition. This enables us to compute the flow expansion to arbitrary order in terms of the initial conditions at final time t. While straightforward to implement, the DA integration method can be very time consuming if the right hand side of the ODE is stiff. In particular, in the case of the long term evolution in perturbed 2-body dynamics the fast near-Keplerian motion requires small step sizes. This is not specific to DA but a property found in numerical ODE integration in general. This observation gives rise to the averaging technique described in the next section, which mitigates the impact of this problem by removing the fast motion and replacing it by a smooth mean motion.

IV. AVERAGED DYNAMICS

The orbit evolution in the Earth environment can be expressed in terms of variation of orbital parameters through variational equations in Gauss' form or Lagrange's form [18].

When the long-term propagation of the dynamics is required, it is convenient to separate the disturbing function (or disturbing force) in terms of its constant component, short period variations and long period variations. In particular, it is possible to isolate the secular and the long-period effects on the dynamics by eliminating the short period term through the averaging technique. The most common form is obtained by averaging the perturbation over one orbit revolution. Considering that the evolution of the semi-major axis a, eccentricity e, inclination i, anomaly of the ascending node Ω and anomaly of the pericenter ω are much slower than the true anomaly ν or mean anomaly M, the variational equations can be integrated on ν or M from 0 to 2π, considering the other orbital elements constant over one revolution. The averaged dynamics can then be numerically integrated to account for the variation of the orbital elements over the long period. The osculating terms can also be retried a posteriori.

In this article we consider the effects of some of the main perturbations for Earth-centered orbits including solar radiation pressure, the effect of the Earth's oblateness and luni-solar perturbations. The expression for the averaged potential to describe the long-term and secular variation of the orbital elements were derived in [4] and [6], we summarize the main point here for clarity.

The secular and long-period rate of change of the orbital elements due to solar radiation pressure (SRP) and J_2 are given for example by Krivov et al. [3] and were implemented in the PlanODyn suite [8] as:

$$\begin{aligned}
\frac{d\overline{\Omega}}{dt}_{J_2} &= -\frac{3}{2}J_2\left(\frac{R_E}{a}\right)^2\frac{n}{(1-e^2)^2}\cos i \\
\frac{d\overline{\omega}}{dt}_{J_2} &= \frac{3}{4}J_2\left(\frac{R_E}{a}\right)^2\frac{n}{(1-e^2)^2}\left(5\cos^2 i-1\right) \quad (4)
\end{aligned}$$

for the Earth oblateness, where $J_2 = 1.083\cdot 10^{-3}$, R_E is the radius of the Earth and n the orbital mean motion, and

$$\begin{aligned}
\frac{d\bar{e}}{dt}_{SRP} &= \frac{3}{2}\frac{na_{SRP}a^2}{\mu}\sqrt{1-e^2}\sum_{k=1}^{6}A_k\sin\alpha_k \\
\frac{d\bar{i}}{dt}_{SRP} &= \frac{3}{2}\frac{na_{SRP}a^2e}{\mu\sqrt{1-e^2}}\cos\omega\sum_{k=7}^{9}A_k\sin\alpha_k \\
\frac{d\overline{\Omega}}{dt}_{SRP} &= \frac{3}{2}\frac{na_{SRP}a^2e}{\mu\sin i\sqrt{1-e^2}}\sin\omega\sum_{k=1}^{6}A_k\sin\alpha_k \\
\frac{d\overline{\omega}}{dt}_{SRP} &= -\cos i\frac{d\overline{\Omega}}{dt}_{SRP}+ \\
&\quad \frac{3}{2}\frac{na_{SRP}a^2}{\mu}\frac{\sqrt{1-e^2}}{e}\sum_{k=1}^{6}A_k\sin\alpha_k \quad (5)
\end{aligned}$$

The coefficients A_1 to A_9 and the angles α_1 to α_9 are function of the orbit orientation i, Ω, ω, and the longitude of the Sun on the ecliptic λ_{Sun} as well as the obliquity angle ε of the ecliptic over the equator. a_{SRP} is the characteristic acceleration due to SRP:

$$a_{SRP} = \frac{p_{SR}c_R A}{m} \quad (6)$$

with p_{SR} the is the solar pressure $p_{SR} = 4.56\cdot 10^{-6}\ N/m^2$, c_R the reflectivity coefficient, and A/m the area-to-mass ratio of the spacecraft with A the cross section area exposed to the Sun. The effect of eclipses is neglected for the moment. The secular variation of semi-major axis due to Earth's oblateness and solar radiation pressure without considering eclipses is zero. The effect of the third body perturbation due to the Moon and the Sun is also considered, by averaging the third body potential written in orbital elements. The expression of the resulting equations are reported in [6].

For integrating DA with SA techniques, the algorithm implemented in PlanODyn was implemented in COSY INFINITY. The COSY implementation was successfully validated against the PlanODyn implementation of both the averaged dynamics and the high-fidelity dynamics. For the high fidelity dynamics the expression of the acceleration due to Solar radiation pressure, Earth's oblateness and luni-solar perturbation were inserted into the Gauss's form of planetary equations [18] to be numerically integrated.

V. DENSITY PROPAGATION

The term *density* may refer to both a physical density as well as a probability density function (pdf) in the phase space of a given dynamical system. The physical density $N(\boldsymbol{x})$ gives the number of particles in the system that occupy an infinitely small phase space volume around the state

$\boldsymbol{x}$. The probability density function $p(\boldsymbol{x})$, on the other hand, provides the probability of a particle occupying an infinitely small phase space volume around the state $\boldsymbol{x}$. Mathematically, both formulations are in fact identical except for normalization. The pdf is normalized such that the total integrated probability of a particle occupying any state is 1,

$$\int_V p(\boldsymbol{x})\, dV = 1,$$

while the physical density is normalized such that the integral yields the total number of particles in the system:

$$\int_V N(\boldsymbol{x})\, dV = N_{tot}.$$

Without loss of generality we shall refer to the density as a pdf for the remainder of this paper.

It is important to note that our notion of density in phase space differs from the notion of spatial density. The spatial density is the density of particles in physical space only, neglecting different velocities present in phase space. In order to pass from the phase space density to the spacial density, it is necessary to integrate the distribution over the velocity.

In general, as a dynamical system evolves with time, the pdf also changes. Thus, the pdf is time dependent: $p_t(\boldsymbol{x})$. The goal of this section is to obtain a transformation from the known pdf $p_{t_0}(\boldsymbol{x})$ at time t_0 to the general pdf $p_t(\boldsymbol{x})$ at any time t. Fortunately, the evolution of the density in a dynamical system where particles are conserved locally, i.e. a system without sources or sinks of particles, is fully described by the local evolution of phase space volume under the effect of the ordinary differential equation governing the motion.

Let the evolution of a dynamical system be described by the first order ordinary differential equation

$$\frac{d\boldsymbol{x}}{dt} = f(\boldsymbol{x}, t), \tag{7}$$

where $f : \mathbb{R}^n \to \mathbb{R}^n$ is a C^1 function, i.e. at least once continuously differentiable, and $\boldsymbol{x}(t) \in \mathbb{R}^n$ is the state vector of the system. For any given initial condition $\boldsymbol{x}_0$ at time t_0, this ODE has a unique solution $\boldsymbol{x}(t)$ such that $\boldsymbol{x}(t_0) = x_0$ and $\boldsymbol{x}(t)$ satisfies Eq. 7.

We define $\varphi_t(\boldsymbol{x})$ to be the general solution of the ODE defined by Eq. 7 satisfying

$$\begin{cases} \varphi_{t_0}(\boldsymbol{x}) &= \boldsymbol{x} \\ \frac{d\varphi_t(\boldsymbol{x})}{dt} &= f(\varphi_t(\boldsymbol{x}), t), \end{cases}$$

i.e. $\varphi_t(\boldsymbol{x})$ is the flow of the ODE.

Fixing the time t, $\boldsymbol{y} = \varphi_t(\boldsymbol{x})$ defines a map from any initial point $\boldsymbol{x}$ in phase space at time t_0 to the corresponding final point $\boldsymbol{y}$ in phase space at time t. Due to the uniqueness of solutions of the ODE, this map is a 1-to-1, and hence invertible, C^1 transformation of phase space. We denote the inverse function by $\boldsymbol{x} = \varphi_t^{-1}(\boldsymbol{y})$ and the Jacobian with respect to the phase space variables $\boldsymbol{x}$ and $\boldsymbol{y}$ as $J\varphi_t(\boldsymbol{x})$ and $J\varphi_t^{-1}(\boldsymbol{y})$ respectively.

The problem of obtaining the relationship between $p_t(\boldsymbol{x})$ and $p_{t_0}(\boldsymbol{x})$ now is reduced to finding the pdf of the dependent variable $\boldsymbol{y} = \varphi_t(\boldsymbol{x})$ given the pdf of $\boldsymbol{x}$. This relation between

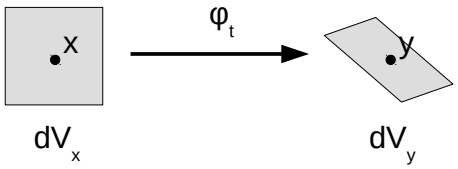

Figure 2: Illustration of the transformation of an infinitesimal volume dV_x to dV_y under the map φ_t.

the pdf of a dependent and independent variable is well known in statistics [19, p. 149] and given by

$$p_t(\boldsymbol{y}) = p_t\left(\varphi_t^{-1}(\boldsymbol{y})\right) \cdot \det\left(J\varphi_t^{-1}(\boldsymbol{y})\right), \tag{8}$$

or written in terms of $\boldsymbol{x}$

$$p_t\left(\varphi_t(\boldsymbol{x})\right) = p_t\left(\boldsymbol{x}\right) / \det\left(J\varphi_t(\boldsymbol{x})\right). \tag{9}$$

In the second equation we made use of the fact that $J\varphi_t^{-1}(\boldsymbol{y}) = \left(J\varphi_t(\boldsymbol{x})\right)^{-1}$ and hence

$$\det\left(J\varphi_t^{-1}(\boldsymbol{y})\right) = 1/\det\left(J\varphi_t(\boldsymbol{x})\right).$$

Equations 8 and 9 can be understood intuitively by considering the evolution of infinitesimally small phase space volumes. To derive Eq. 9, consider the infinitesimally small phase space volume dV_x centered around $\boldsymbol{x}$. Mapping this infinitesimally small phase space volume dV_x forward through the map φ_t yields another infinitesimally small phase space volume dV_y centered around $y = \varphi_t(\boldsymbol{x})$ (see Figure 2).

The probability of a particle occupying the phase space volume dV_x at time t_0 is given by $p_{t_0}(\boldsymbol{x}) \cdot dV_x$, while the probability of a particle occupying dV_y at time t is given by $p_t(\boldsymbol{y}) \cdot dV_y = p_t(\varphi_t(\boldsymbol{x})) \cdot dV_y$. Due to the principle of probability conservation, both probabilities must be the same, yielding

$$p_{t_0}(\boldsymbol{x}) \cdot dV_x = p_t(\varphi_t(\boldsymbol{x})) \cdot dV_y.$$

Solving for $p_t(\varphi_t(\boldsymbol{x}))$ we obtain

$$p_t(\varphi_t(\boldsymbol{x})) = p_{t_0}(\boldsymbol{x}) \cdot dV_x/dV_y. \tag{10}$$

Drawing on a result from differential geometry, we recall that the relation between the initial volume dV_x and the final volume dV_y is given by

$$dV_y = \det\left(J\varphi_t(\boldsymbol{x})\right) \cdot dV_x, \tag{11}$$

where the quantity inside the determinant is also known as the Riemann or metric tensor [20, p. 159]. Inserting Eq. 11 into Eq. 10 we obtain Eq. 9.

VI. DA IMPLEMENTATION

As the result of the preceding section, we obtained the relationship between the densities at different times in a dynamical system given by Eq. 9. In order to compute the new pdf $p_t(\varphi(\boldsymbol{x}))$, this equation requires the computation of the determinant of the metric tensor $\det\left(J\varphi_t(\boldsymbol{x})\right)$. This in turn requires knowledge of the derivatives of the flow to obtain the Jacobian $J\varphi_t(\boldsymbol{x})$.

While it is of course possible to manually derive the variational equations corresponding to the particular given dynamics and integrate the combined equations of motion in order to obtain the Jacobian $J\varphi_t(\boldsymbol{x})$ at the given point, this process has several drawbacks. Firstly, it requires the manual derivation of the variational equations for each and every different ODE. Given the complexity of many more realistic dynamical models, this task can become quite tedious and yield very long and difficult expressions. Furthermore, even for a simple 6 dimensional phase space, the dimensionality of the ODE including the variational equations is already 42, resulting in significant additional computational effort. Lastly, this procedure only provides the Jacobian and hence the new density at a single point. In order to evaluate the density at many different points, e.g. in a cloud of initial conditions, a separate integration is required for every single evaluation.

We instead use DA to compute an expansion of the new density as given in Eq. 9 without the need of manually taking and integrating derivatives. We achieve this by making use of the differential structure of DA. First, a high order flow expansion between times t_0 and t is computed as described in section III. Since the final result of this process is a polynomial expansion of $\varphi_t(\boldsymbol{x})$ in terms of $\boldsymbol{x}$, it is easy to take the derivative of the polynomial expansion to obtain a polynomial expansion of the Jacobian $J\varphi_t(\boldsymbol{x})$.

Performing all the operations in the computation of the metric tensor in DA arithmetic, followed by the DA evaluation of the determinant itself, one obtains an expansion of the determinant of the metric tensor. This then allows the fast and efficient evaluation of the density $p_t(\varphi_t(\boldsymbol{x}))$ by Eq. 9. As the determinant itself is a polynomial expansion valid in an entire neighborhood of the chosen expansion point, it is possible to evaluate the density $p_t(\varphi_t(\boldsymbol{x}))$ not just at the expansion point itself, but at any number of points in its neighborhood without the need for additional integrations by the simple evaluation of a polynomial.

Note that we do not compute the full Taylor expansion of the final pdf $p_t(\varphi_t(\boldsymbol{x}))$. Instead, we leave the explicit dependence on the initial pdf $p_{t_0}(\boldsymbol{x})$ as per Eq. 9 intact. This has several advantages. Firstly, it is possible to propagate a different pdf without reintegrating the dynamics to recompute the metric tensor. Secondly, expanding the entire pdf directly will typically result in an expansion with poor convergence as the pdf has an asymptotic behavior approaching zero, while all non-trivial polynomials of course diverge to $\pm\infty$. Thus a single polynomial expansion will only describe the pdf well only in a small, local neighborhood, which for typical pdfs (such as Gaussian distributions) is much smaller than the radius of convergence of the determinant.

We further remark that the above method is applicable also to the computation of the density as given in Eq. 8. The only difference is that in this case the numerical integration is to be carried out backwards from time t to time t_0, starting with a DA initial condition $[\boldsymbol{y}]$ at time t to obtain the DA expansion of the expression $\left[\varphi_t^{-1}\right](\boldsymbol{y})$.

Which of the two formulations, Eq. 8 or 9 to calculate is largely problem dependent. Either representation of the pdf has advantages depending on the final goal that is to be achieved with the pdf. In the following section, we compute the density according to Eq. 9, expanding around the area of interest in the prescribed initial density distribution $p_{t_0}(\boldsymbol{x})$. For visualizing the final pdf, this formulation is ideal as it at the same time shows the evolution of the initial set in phase space over time, while in addition providing the density at each point in the propagated set.

VII. NUMERICAL EXAMPLES

To demonstrate the proposed method of DA-based propagation of the phase space density in semi-analytical dynamics, we consider an initial condition on a Medium Earth Orbit characterized by the values given in Tab. 1. Objects with high area-to-mass ratio A/m equal to 25 m^2/kg are considered. The set of initial conditions used in the following propagations is centered around the reference values, with the size in each component as given. As can be seen, in this study we only consider two dimensional statistics in e and ω, while the other elements are considered exact. This is not a restriction of the method but merely serves to simplify the representation of the resulting probability density function in phase space.

In the following, to increase the clarity of the explanation of the cloud evolution, a dynamical model with increasing complexity is used. First, a simplified Sun model is adopted as in [3] and [4]: the ecliptic plane is assumed to be equivalent to the equatorial plane (i.e., obliquity angle $\varepsilon = 0$) and the Earth is assumed on a circular orbit around the Sun. The only perturbations considered are solar radiation pressure and J_2. This will reveal some interesting characteristics of the phase space map as first noted in [12]. Then the model complexity is increased by considering the real ephemerides of the Sun as well as including in the model luni-solar perturbations using a second-degree model of the disturbing potential.

Element	Reference	Size
a_0	23222 km	± 0 km
e_0	0.08	± 0.03
i_0	0.01 deg	± 0 deg
Ω_0	0 deg	± 0 deg
ω_0	0 deg	± 5.7 deg
M_0	0 deg	± 0 deg

Table 1: Initial conditions used for the propagations.

VIII. J_2 AND SIMPLIFIED SRP DYNAMICS

The two-body dynamics of a spacecraft with high area-to-mass ratio orbiting the Earth is strongly perturbed by the term of the gravitational field due to the Earth's oblateness and by the effect of solar radiation pressure in the case of large area-to-mass ratio.

The orbit evolution shows interesting behavior in the phase space of eccentricity e and ϕ, where

$$\phi = \Omega + \omega - (\lambda_{Sun} - \pi)$$

describes the orientation of the orbit perigee with respect to the Sun. As was analyzed in [4], if the obliquity angle is assumed to be zero, the system allows some equilibrium solutions which correspond to frozen orbits with resect to the Sun. The equilibrium solution $\phi = 0$, existing at semi-major axis below approximately 15000 km corresponds to a family of heliotropic orbits that maintain their perigee in the direction of the Sun, while $\phi = \pi$, existing for semi-major axis above 13000 km approximately, corresponds to families of anti-heliotropic orbits, with the apogee frozen in the Sun direction.

Initial conditions around the equilibrium orbit will librate in the phase space of $e-\phi$ around the equilibrium. The eccentricity value of the equilibrium solution depends on the semi-major axis a and the value of the area-to-mass ratio A/m of the spacecraft, which can be used as a control parameter to design frozen orbits with respect to the Sun. A detailed description of the possible solutions is given in [4].

In this simplified model we study the evolution of the density under a simplified solar ephemeris model and the effect of J_2 and solar radiation pressure only. As mentioned, the equator is assumed to be on the ecliptic, $\varepsilon = 0$ and a circular orbit for the Earth around the Sun is used. Instead of studying the motion in full six dimensional phase space, we focus on the projection into the $e - \phi$ plane.

Figure 3 shows the evolution of an initial set of phase space with initially uniform density (bottom). As the system evolves, the set moves counter clockwise on a periodic orbit. The period of the motion is about 378.3 days. Note that the period of the motion, i.e., one librational loop around the equilibrium point (which corresponds to an anti-heliotropic orbit), should not be confused with the orbit period. Unless otherwise stated we will refer here to the librational loop period. As can be seen, the phase space is compressed during the evolution. However, the compression is not uniform over the initial set, causing the density to become significantly non-uniform over the initial set. After completing one full period, the set returns almost to the initial set and also the density almost returns to the initial uniform distribution.

Figure 4 shows the evolution of the minimum and maximum densities at various times during one single loop period. Starting from the uniform distribution of (non-normalized) density 1, both the minimum and the maximum density increases, but after about half a period the difference between the minimum and maximum density becomes largest. On the second half period, the difference between the minimum and maximum density decreases again and approaches almost the initial density.

The same effect is visible also over several turns. In Figure 5 the evolution over three complete periods is shown. The periodic expansion and compression of the density and in particular the non-uniform density evolution within the initial set during a single period is clearly visible.

From the previous figures it appears as if the density is changing periodically. In case of only solar radiation pressure in this model, this is indeed the case as was shown by an analytical analysis of the Hamiltonian of that system as a consequence of Liouville's theorem [12]. In case of the presence of

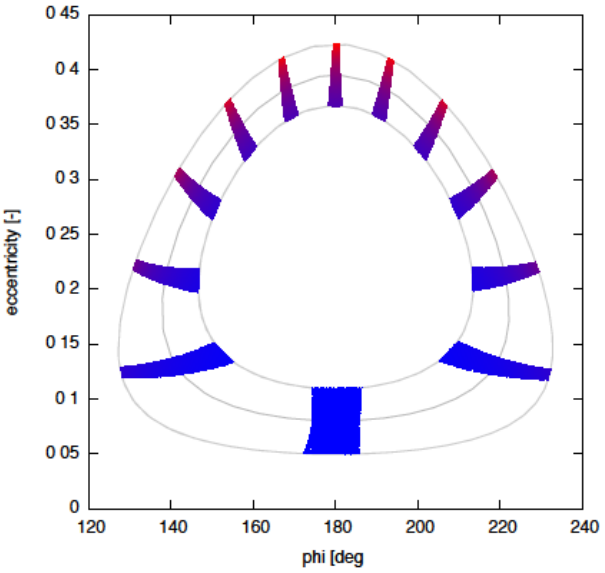

Figure 3: Phase space evolution of initial set with uniform density over one loop period.

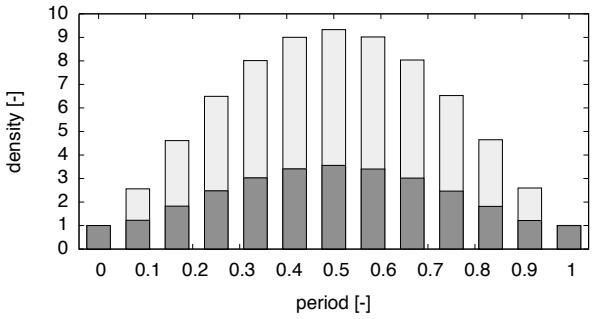

Figure 4: Evolution of the minimum and maximum density over one period.

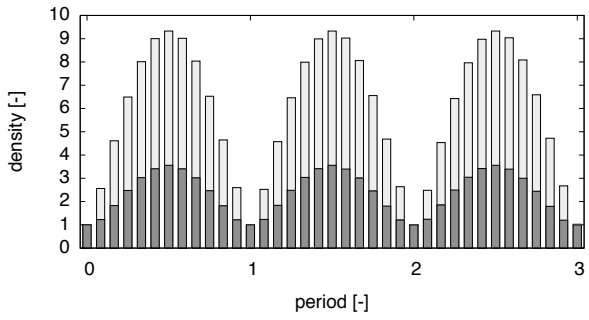

Figure 5: Evolution of the minimum and maximum density over three periods.

J_2, however, this is not the case, as a more careful long term analysis shows. In Figure 6 we show the minimum and maximum density after each completed period for 15 periods. In this representation, which is ignoring the intermediate pulsating density evolution during each period, it becomes apparent that the minimum and maximum density in each turn is indeed drifting apart with time.

In Figure 7 the reason for this evolution becomes clear. As the initial set evolves, different parts move at different speeds

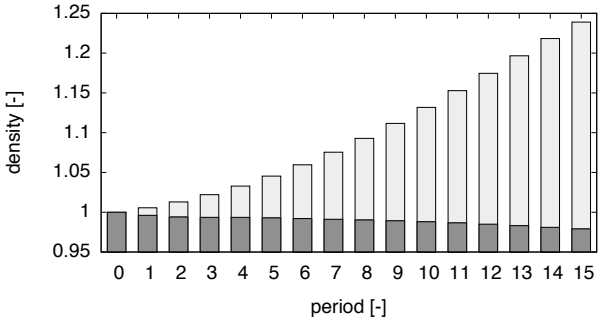

Figure 6: Long term evolution of the minimum and maximum density after each period.

resulting in a more and more non-linear shape and less uniform density distribution. Note that even in this case a single polynomial expansion is sufficient to accurately represent both the shape in phase space as well as the density of the cloud. This demonstrates the power of the DA density propagation method even under long term evaluation.

Also in terms of computational cost, this method is highly effective. The figures displayed here are generated by propagating $10,000$ random samples within the initial condition box, and propagating them forward, in the case of Figure 7 for over 15.5 years. During the integration, snapshots of the position and density are taken at fixed intervals to generate the intermediate results. The computational time required for any one of these computations is on the order of tens of seconds on an ordinary iMac with an 2.9 GHz Intel Core i5 processor and 8 GB DDR3 RAM.

Lastly, Figures 8 and 9 show the evolution of a non-uniform initial density distribution. In the first figure, a single Gaussian density distribution in both ϕ and e is placed in the center of the initial condition box (centered at $\phi = \pi$ and $e = 0.08$). In the second figure, two initially identical Gaussians are placed each $1/8$ away from the top and bottom respectively of the initial condition box (centered at $\phi = \pi$ rad and $e = 0.0575$ and $e = 0.1025$, respectively). As can be seen in Figure 9, the density of the two Gaussians evolves differently as the density of the outer Gaussian increases significantly more than the density of the inner Gaussian.

IX. J_2, SRP AND FULL LUNI-SOLAR DYNAMICS

Once the phase space evolution is clear we can now replace the simplified model of the dynamics with a more accurate model including perturbations due to J_2, SRP and the luni-solar gravitational potential using real ephemeris data for the Sun and Moon. The obliquity angle of the ecliptic over the equator is set to $\varepsilon = 23.4393$ deg and the real ephemerides of the Earth around the Sun as well as the Moon around the Earth are considered, based on a low order polynomial analytical model.

As Figure 10 shows, including luni-solar perturbations and a more realistic ephemeris of the Sun leads to non-periodic motion. However, the DA method for density propagation is working the same way as before without changes to the code after changing the dynamical model. The additional

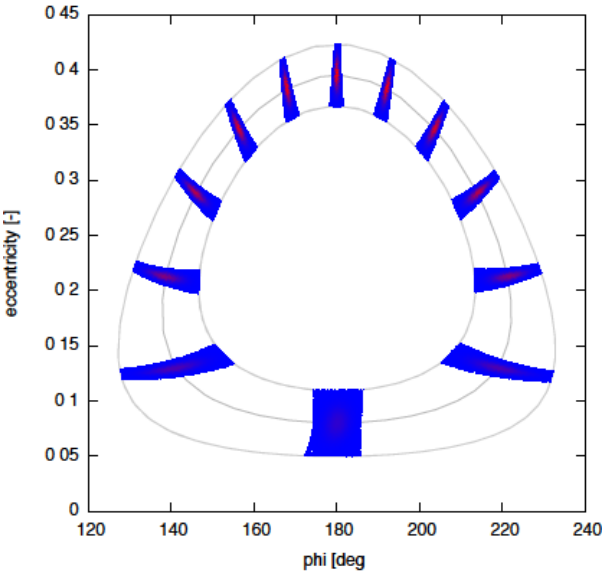

Figure 8: Density evolution of a non-uniform Gaussian density distribution.

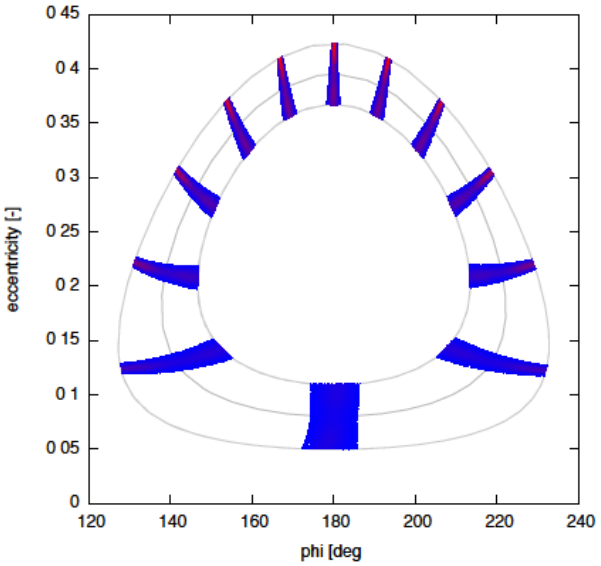

Figure 9: Density evolution of a non-uniform and non-Gaussian initial density.

terms in the dynamical model do not require any further work for the density propagation.

X. CONCLUSIONS

In this paper, we introduced a DA based method for the propagation of sets of initial conditions in phase space and their associated phase space densities, and then applied this technique to a DA enabled implementation of SA dynamics.

The DA based method for the propagation of densities introduced in this paper is independent of the dynamical system, and can be applied to both averaged (SA) as well as non-averaged (high fidelity) dynamics. However, the particular combination of DA techniques with SA equations yields a fast

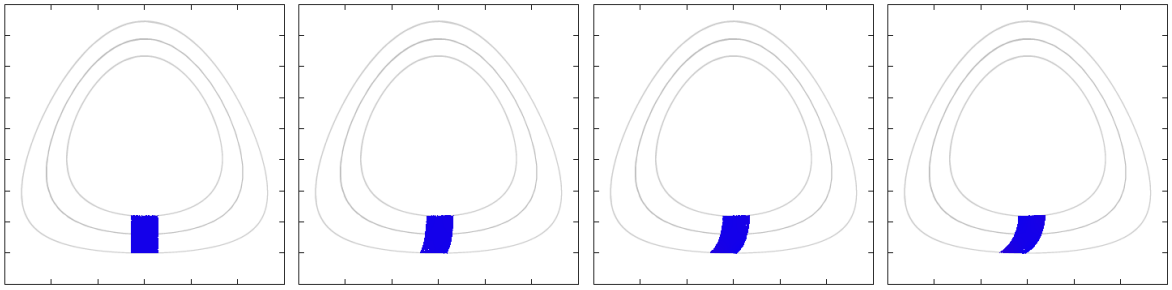

(a) initial set (b) period 1 (c) period 2 (d) period 3

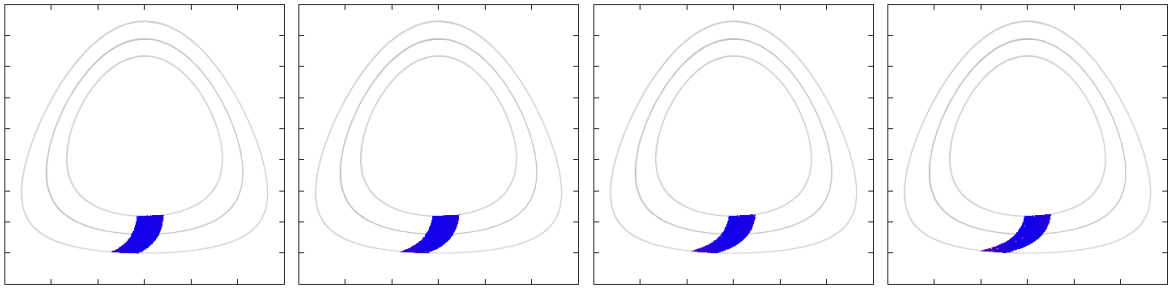

(e) period 4 (f) period 5 (g) period 6 (h) period 7

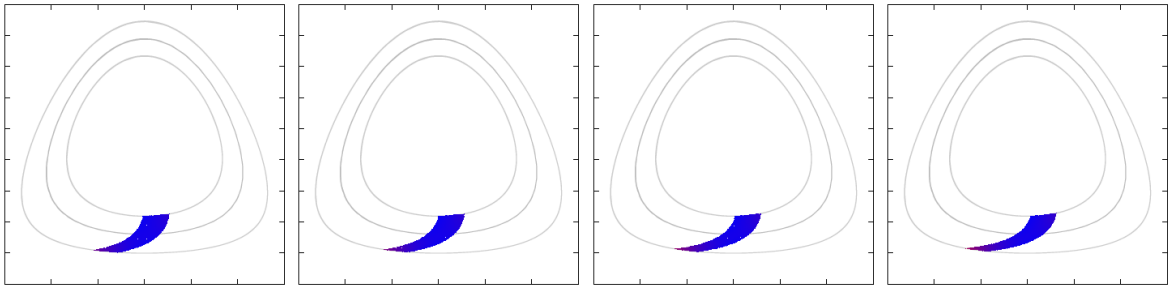

(i) period 8 (j) period 9 (k) period 10 (l) period 11

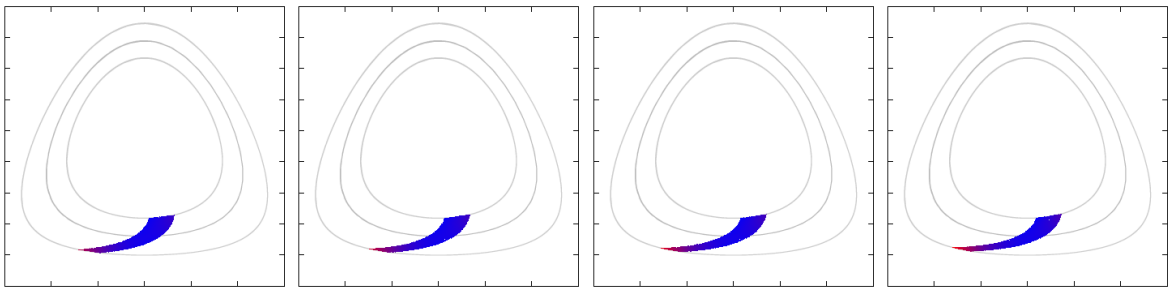

(m) period 12 (n) period 13 (o) period 14 (p) period 15

Figure 7: Long term evolution of initial set with uniform density distribution after every period.

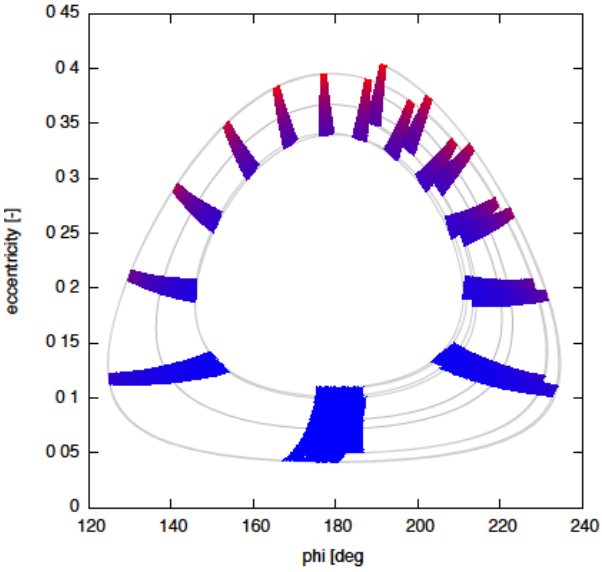

Figure 10: Phase space evolution of initial set with uniform density over one period.

and accurate method to propagate large clouds of initial conditions and their associated probability density functions very efficiently for long time.

The evolution of a cloud of high area-to-mass objects in MEO is reproduced considering the effects of solar radiation pressure, the Earth's oblateness and luni-solar perturbation. The computational efficiency is demonstrated by propagating $10,000$ random samples taking snapshots of the position and density at each point throughout the integration. The time required for an integration of 16 years is on the order of seconds on an ordinary desktop PC.

As a future work, coupling the expression of the density in the phase space with the density over one single orbit (derived under a two-body approximation), will allow recovering the full 6D density of high area-to-mass objects lost due to the averaging over the fast variable M. This opens the door for applications to the description of debris evolution.

Moreover, the coupling or DA mapping with SA techniques will be investigated as an alternative to double averaged techniques and the DA domain splitting will be employed in some case where the dynamics exhibit strongly nonlinear behavior in the chaotic regime.

ACKNOWLEDGMENTS

A. Wittig gratefully acknowledges the support received by the Marie Curie fellowship PITN-GA 2011-289240 (AstroNet-II). C. Colombo acknowledges the support received by the Marie Curie grant 302270 (SpaceDebECM - Space Debris Evolution, Collision risk, and Mitigation) within the 7^{th} EU Framework Programme.

REFERENCES

[1] R. Armellin, P. Di Lizia, F. Bernelli Zazzera, and M. Berz. Asteroid close encounter characterization using differential algebra: the case of aphophis. *Celestial Mechanics and Dynamical Astronomy*, 107(4), 2010.

[2] M. Valli, R. Armellin, P. Di Lizia, and M. Lavagna. Nonlinear management of uncertainties in celestial mechanics. In *AAS/AIAA Space Flight Mechanics Meeting, Charleston, SC*, number AAS 12-264, 2012.

[3] A. V. Krivov, L. L. Sokolov, and V. V. Dikarev. Dynamics of mars-orbiting dust: Effects of light pressure and planetary oblateness. *Celestial Mechanics and Dynamical Astronomy*, 63(3):313–339, 1995.

[4] C. Colombo, C. Lücking, and C. McInnes. Orbital dynamics of high area-to-mass ratio spacecraft with J_2 and solar radiation pressure for novel earth observation and communication services. *Acta Astronautica*, 81(1):137–150, 2012.

[5] A. Rossi, L. Anselmo, A. Cordelli, P. Farinella, and C. Pardini. Modelling the evolution of the space debris population. *Planetary and Space Science*, 46(11-12): 1583–1596, 1998.

[6] C. Colombo. Semi-analytical propagation for highly elliptical orbits to build maps for end-of-life disposal. In *Key Topics in Orbit Propagation Applied to SSA - KePASSA, April 23-25, Logroño, Spain*, 2014.

[7] A. Wittig, R. Armellin, C. Colombo, and P. Di Lizia. Long-term orbital propagation through differential algebra transfer maps and averaging semi-analytical approaches. In *AAS/AIAA Space Flight Mechanics Meeting, Santa Fe, NM*, number AAS 14-224, 2014.

[8] C. Colombo, F. Letizia, E. M. Alessi, and M. Landgraf. End-of-life earth re-entry for highly elliptical orbits: the integral mission. In *AAS/AIAA Space Flight Mechanics Meeting, Santa Fe, NM*, number AAS-14-325, 2014.

[9] C. R. McInnes. An analytical model for the catastrophic production of orbital debris. *ESA Journal*, 17(4):293–305, 1993.

[10] F. Letizia, C. Colombo, and H. G. Lewis. Analytical model for the propagation of small debris objects clouds after fragmentations. *Journal of Guidance, Control, and Dynamics*, 2014.

[11] N. Gor'kavyi. A new approach to dynamical evolution of interplanetary dust. *The Astrophysical Journal*, 474 (1):496–502, 1997.

[12] C. Colombo and C. R. McInnes. Evolution of swarms of smart dust spacecraft. In *New Trends in Astrodynamics and Applications VI, New York, June 2011*, 2011.

[13] M. Berz. *Modern Map Methods in Particle Beam Physics*. Academic Press, 1999.

[14] M. Berz. *The new method of TPSA algebra for the description of beam dynamics to high orders*. Los Alamos National Laboratory, 1986. Technical Report AT-6:ATN-86-16.

[15] M. Berz. The method of power series tracking for the mathematical description of beam dynamics. *Nuclear Instruments and Methods A258*, 1987.

[16] M. Berz. *Differential Algebraic Techniques, Entry in Handbook of Accelerator Physics and Engineering*. World Scientific, New York, 1999.

[17] M. Berz and K. Makino. *COSY INFINITY version 9 reference manual*. Michigan State University, East Lansing, MI 48824, 2006. MSU Report MSUHEP060803.

[18] R.H. Battin. *An Introduction to the Mathematics and Methods of Astrodynamics*. AIAA Education Series, Reston, VA, 1999.

[19] T.T. Soong. *Fundamentals of Probability and Statistics for Engineers*. Wiley, 2004. ISBN 9780470868133. LCCN 2004041235.

[20] M. M. Postnikov. *Geometry VI: Riemannian Geometry*, volume 91 of *Encyclopaedia of Mathematical Sciences*. Springer, 2001. ISBN 9783540411086.